IMPACT OF IMPERFECT CHANNEL ESTIMATION AND ANTENNA CORRELATION ON QUANTISED MASSIVE MIMO SYSTEMS

A PREPRINT

Murat Temiz, Emad Alsusa,Laith Danoon

ABSTRACT

This paper examines the uplink performance of large-constellation multi-user massive MIMO systems with low-resolution analogue-to-digital converters (ADCs) in the presence of channel correlation and imperfect channel state information (CSI). The base station (BS) employs a large number of antennas for multiplexing and demultiplexing co-channel users with each antenna element having a dedicated radio frequency (RF) chain and two low-resolution ADCs. While such ADCs cause data loss due to coarse quantization, the large number of antennas can be exploited not only to alleviate such a problem but also to make it possible to utilise large-constellation modulation schemes. The results provide an insight into the trade-off between various performance metrics and the number of quantization bits under a wide range of realistic conditions. It will be shown that 1-bit quantization provides sufficient resolution with 100 BS antennas to communicate with 10 UEs using QPSK, but the number of quantization bits must be increased for larger constellations particularly to overcome CSI mismatch and channel correlation. The results also consider the trade-off between average mutual information and power consumption of the low-resolution ADCs. It will be shown that 16QAM with 2-bit quantization may provide a good compromise between energy efficiency and average mutual information.

1 Introduction

Multi-user massive MIMO is expected to play an important role in future wireless communication systems due to its ability to increase power and spectral efficiencies as well as the reliability of the network [1]. In such systems, the base station (BS) employs many antennas, each of which is connected to separate RF chains, ADCs and digital-to-analogue converters (DACs). Due to this significant amount of hardware usage per antenna; the complexity, cost and the energy consumption of the hardware scale up with the number of BS antennas. To counter this, low-resolution ADCs for the uplink and low-resolution DACs for the downlink are preferred. The application of such low-resolution devices significantly reduces hardware cost, energy consumption and the binary sample size, hence the required signal processing power.

In massive MIMO systems, the BS antennas receive signals from all UEs at the same time-frequency resources. Subsequently, the received signals by each antenna port are processed separately through RF chains which convert high-frequency RF signals to baseband signals and reconstruct I and Q components of them (IQ demodulation). Afterwards, the received baseband analogue signals must be digitised by ADCs before performing digital signal processing in order to equalise and demodulate the signals and acquire the transmitted messages. Therefore, ADCs are paramount parts of the system and their energy consumption must be taken into account. Various studies have recently investigated the application of 1-bit and low-resolution ADCs on the massive MIMO uplink using non-linear (capacity achieving) or linear (sub-optimal) receivers [2-7]. The minimum energy consumption of ADCs increases exponentially with the resolution and increases proportionally with the sampling rate [8] which must be at least $2f_{max}$ in accordance with the Nyquist criteria. However, ADCs operate at higher sampling rates to provide enough samples for the demodulation

[1]Note: This research article has been accepted to be published in IET Communications, however, this is not the published version of the paper. Please view the published version of the article in IET or IEEE databases.

of high-order modulated signals in most communication systems. Although recent advancements in the fabrication of semiconductors devices have led to the production of highly efficient integrated circuits, high-resolution ADCs for RF systems still consume relatively much higher energy than their low-resolution counterparts, especially at high sampling rates. Therefore, keeping their resolutions as low as possible without causing performance degradation on the communication link is essential to optimise the energy consumption of the receiver circuits. Reduced ADC resolution also decreases the computational power requirements and energy consumption of the connected subsequent digital signal processing units due to the decreased amount of ADC output data. Accordingly, implementing low-resolution ADCs would significantly contribute to the optimisation of the BS hardware in terms of energy efficiency and complexity.

Employing 1-bit ADCs has been researched extensively for communication systems with oversampling in [9] and without oversampling in [10]. Since the architecture of 1-bit ADCs is very simple and does not require any automatic gain control unit (AGC), they are especially attractive for massive MIMO systems, due to the fact that the real and imaginary parts of the received baseband signals from each antenna port needs to be quantized separately, and this significantly increases the required number of ADCs. The performance of 1-bit ADCs for massive MIMO uplink is investigated in [2-5], in which it has been shown that QPSK demodulation can be realised using 1-bit ADCs while the BS is receiving signals simultaneously from multiple UEs. On the other hand, it is not possible to effectively perform 16-QAM demodulation with 1-bit ADCs to communicate with multiple UEs [4]. Furthermore, channel estimation with 1-bit ADCs requires very long training (pilot) sequences because coarse quantization destroys a significant amount of information in the received signals [6]. It was shown that at least 2.2 times more antennas are necessary with 1-bit resolution to achieve the performance of high-resolution ADCs [7] which also renders 1-bit ADCs insufficient for the demodulation of higher order modulated signals as it would result in using more RF chains.

Low-resolution quantized massive MIMO uplink is investigated in [11], where it is shown that 16-QAM or higher order modulation schemes require more than 1-bit resolution assuming ideal channel conditions and no correlation effects.

The non-line-of-sight (NLOS) channel is favourable for MIMO systems due to its scattering which enriches diversity, hence decreases the correlation between channels. The best scenario is said to be when the channel matrix is assumed to consist of independent and identically distributed (i.i.d.) random complex values as then the channels would be entirely independent. However, it is unlikely to achieve such favourable channel conditions in practical scenarios due to the fact that the antennas must be placed in a limited space at the BS, and the UEs may be located close to each other. These situations give rise to channel correlation and which will degrade the performance as shown theoretically and through channel measurements in [12, 13]. Channel correlation was explored for various antenna array geometries in [12]. Several downlink channel measurements are carried out using $64-$ element antenna arrays with three different arrangements (64×1 vertical array, 1×64 horizontal array, and 8×8 rectangular planar array) with $\lambda/2$ distance between adjacent antenna elements. Measurement results show that the horizontal arrangement outperforms other geometries and may have similar characteristics with the i.i.d. channel [12]. Antenna correlation has a significant impact on the throughput of the system as demonstrated in [13] in which severe degradation is observed when the correlation coefficient is greater than 0.6 ($\phi > 0.6$). Furthermore, the joint impact of mutual coupling and spatial correlation on large-scale MIMO transmitters are investigated in [14]. Modelling of the channel correlation is a challenging task as it is dictated by various parameters such as the distance between antenna elements, the location of the UEs and the

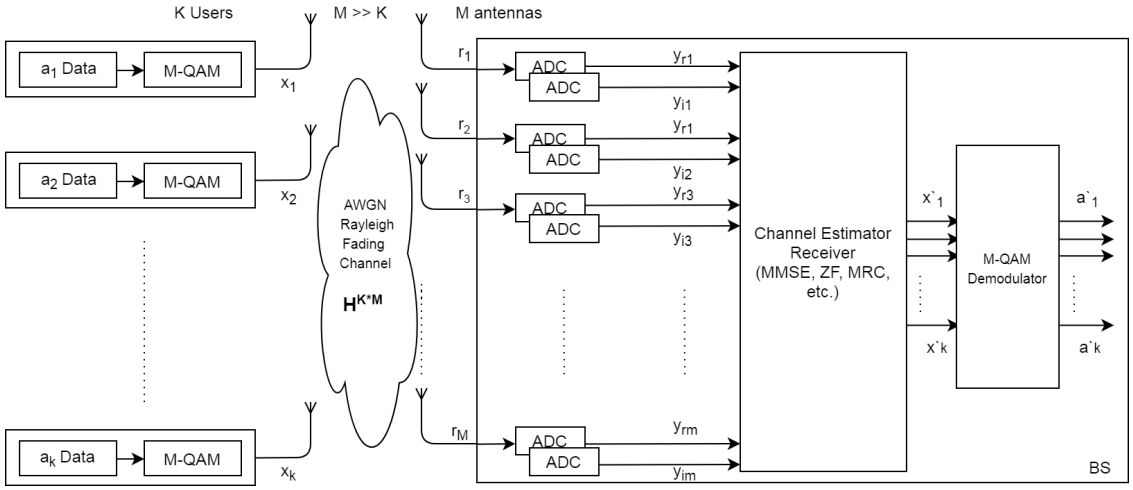

Figure 1: The simplified block diagram of the quantized massive MIMO uplink through a correlated $\mathbf{H}$ channel.

propagation environment. The Kronecker product correlation model based on the ray-based 3D channel model was proposed in [15]. This model utilises the channel separability which corresponds to that horizontal (azimuth) and vertical (elevation) correlation matrices can be determined separately, then the full correlation matrix can be estimated by the Kronecker product of these matrices.

Equally as devastating, CSI mismatch, which is the result of channel estimation errors, causes performance degradation in MIMO systems. Although various techniques have been proposed for channel estimation, the most practical ones are the linear techniques since they tend to have low complexity and can provide similar performance to non-linear techniques in realistic channel conditions. Linear channel estimators such as the least square (LS) estimator and the minimum mean squared error estimator (MMSE) employ pilot symbols for the estimation, hence some frequency or time resources must be allocated for the pilot symbols. During the channel estimation period, CSI mismatch could arise due to mobility of the UEs, hardware mismatches, noise, inter-channel interference errors (ICI) and interpolation errors on pilot symbols. In TDD (time division duplex) systems, further CSI estimation errors could arise due to the distinctnesses between the transmitter and the receiver RF circuits as well as interference differences between the uplink and downlink [16].

1.1 Contributions

1. This study investigates the impact of channel correlation and CSI mismatch on quantized massive MIMO uplinks and provides an insight into the trade-off between spectral and energy efficiency. It also presents an analytical capacity upper bound for the zero forcing (ZF) receiver under the aforementioned channel and hardware conditions.
2. It compares uniform linear (1D) and uniform rectangular (2D) antenna arrays in terms of their effects on the channel correlation by extending the exponential correlation model [17, 18] to cover uniform rectangular arrays.
3. It explores the performance of the square root raised cosine (SRRC) filter and demonstrates that even with 1-bit ADCs, the SRRC can enhance the system performance.
4. It analyses the energy consumption of the ADC blocks as a function of their resolutions and sampling rates with the objective to identify the optimum modulation scheme for each ADC resolution.

1.2 Notation

We use bold lower case and bold upper case letters to indicate vectors and matrices, respectively. $\Re(.)$ and $\Im(.)$ denote the real and imaginary parts of the signal. $Q_n(.)$ indicates the n-bit quantization function and $sign(.)$ function yields the sign of the signal. $\mathbf{A}^H$ denotes the Hermitian transpose of the $\mathbf{A}$ matrix. $\mathcal{CN}(\mu, \mathbf{\Sigma})$ represents the complex Gaussian distribution with mean μ and covariance matrix $\mathbf{\Sigma}$, and $\mathbb{E}[.]$ denotes the expectation operator.

2 System Model

The massive MIMO network under consideration consists of one BS which simultaneously communicates with K UEs through a Rayleigh fading channel. Massive MIMO systems can operate in either FDD (frequency-division duplex) or TDD modes. However, the TDD mode is favourable over FDD as it requires training symbols only during the uplink due to having reciprocal channel properties at the same frequency. This eliminates redundant pilot signalling. Hence, the TDD mode has been assumed here. An OFDM uplink is considered with each sub-carrier assumed to be subjected to flat fading. The BS is equipped with M antenna elements with each element having a separate RF chain and connected two ADCs, hence the BS has $2 \times M$ ADCs as shown in Fig. 1.

2.1 Uplink Model

During the uplink transmission, K UEs transmit data through the H channel to the BS at the same time and frequency resources. To provide enough spatial diversity to each channel, $M \gg K$ must be satisfied. The data transfer from the UEs to the BS start and finish in the same time block τ_i, hence the received signal vector by the BS from all UEs can be given by

$$\mathbf{y_t} = \sqrt{\mathbf{p_u}}\mathbf{H_t}\mathbf{x_t} + \mathbf{n_t}, \quad t = \tau_1, \tau_2 ..... \tau_i \tag{1}$$

where $\mathbf{x}_t \in \mathbb{C}^{K \times 1}$ and $\mathbf{y}_t \in \mathbb{C}^{M \times 1}$ denote the transmitted signal vectors by all UEs and the received signal vectors by the BS at τ_i time block, respectively. p_u is the average transmit power of each UE. The channel matrix is denoted by

$\mathbf{H}_t \in \mathbb{C}^{M\times K}$, which includes the effects of small-scale fading, large-scale fading and the channel correlation. Let $\hat{\mathbf{H}}$ denote the channel matrix without channel correlation, then it will only consist of the small-scale fading coefficients f_{mk} between the kth user and the mth antenna, and large-scale fading coefficients $\sqrt{\gamma_k}$ which are associated with the path-loss from the kth UE to the antenna array; hence, each element of $\hat{\mathbf{H}}$ can be explicitly shown as $\hat{h}_{mk} = f_{mk}\sqrt{\gamma_k}$ with each of its values being independent and identically distributed (i.i.d.) complex random variables with zero mean and unit-variance, as $\hat{\mathbf{H}} \sim \mathcal{CN}(0, \mathbf{I})$. The channel matrix $\mathbf{H}$ with the channel correlation will then be the product of $\hat{\mathbf{H}}$ and square root of the channel correlation matrix, as $\mathbf{H} = \hat{\mathbf{H}}\sqrt{\mathbf{\Phi}}$. The channel correlation matrix $\mathbf{\Phi}$ will be explained further in subsection 2.3. Vector $\mathbf{n}_t \in \mathbb{C}^M$ denotes the AWGN channel noise which consists of i.i.d. random complex variables with a mean noise μ_n and noise variance σ_n^2.

2.2 Quantization Model

Firstly, the received signal is amplified and then separated into real and imaginary parts of the baseband signal by the RF chains and IQ demodulation blocks. The real and imaginary parts of the received signal from the M antennas are quantized separately, therefore $2 \times M$ ADCs are assumed at the BS. Each ADC includes automatic gain control (AGC) and n-bit quantization unit. $Q_n(y)$ denotes the n-bit quantization function, hence the outputs of n-bit $2 \times M$ ADCs at t time-block are obtained as binary data with regard to the step size $\Delta = \frac{(V_{max}-V_{min})}{2^n}$ and the ADC resolution n. Hence, the n-bit quantized received baseband signal vector will be

$$Q_n(\mathbf{y}_t) = Q_n(\Re(\mathbf{H}_t\mathbf{x}_t + \mathbf{n}_t)) + jQ_n(\Im(\mathbf{H}_t\mathbf{x}_t + \mathbf{n}_t)) + \mathbf{n}_q \tag{2}$$

where $\Re$ and $\Im$ denote the real and the imaginary parts of the signal, receptively, and $\mathbf{n_q} \in \mathbb{C}^M$ denotes the quantization noise vector. 1-bit quantization only take the sign of the signal into account and it does not require an AGC unit. Therefore, 1-bit quantization, Q_1, can be given by

$$Q_1(\mathbf{y}_t) = Q_1(sign(\mathbf{H}_t\mathbf{x}_t + \mathbf{n}_t)) + jQ_1(sign(\mathbf{H}_t\mathbf{x}_t + \mathbf{n}_t)) \tag{3}$$

where $sign(.)$ function returns sign of the signals, consequently, the output of the 1-bit ADCs will be either 1 or -1.

2.3 Channel Correlation Model

Channel correlation is mainly caused by nearly spaced antenna elements and nearby UEs. The correlation becomes stronger when the BS antenna elements are closer to each other, hence at least $\lambda/2$ distance between the antenna elements is advised for large-scale antenna arrays [13] to reduce the correlation and the mutual coupling. At higher frequencies, both antenna size and the distance between them can be reduced significantly due to shorter wavelength. Therefore, massive MIMO antenna arrays may be smaller and more compact in millimetre wave systems (e.g. at 25 GHz or higher frequencies).

Although channel correlation is expected to occur mainly at the BS because of the a large number of antenna elements in a limited space, closely located UEs can also give raise to strong correlation particularly in line-of-sight (LOS) propagation environments. A few studies have reported on the behaviour of channel correlation amongst UEs in LOS and NLOS propagation based on experimental channel measurements data [21, 22]. A maximum channel correlation of higher than 0.9 is observed if the UEs are very close to each other in a LOS environment. This very high correlation situation substantially degrades the capacity of the communication links [21]. On the other hand, the minimum measured correlation is 0.2 in [22], which indicates that the channels are nearly independent of each other. Having a very low correlation allows the network to achieve higher capacity.

Uniform, Bessel and exponential correlation models are most commonly used ones to model the channel correlation in existing studies due to their simplicity and consistency with real measurement results. The Uniform correlation assumes that the correlation among all antenna elements is the same and constant while the Bessel correlation model which, utilises $0th$ order Bessel function, is suitable only for highly dense scattering environments [13]. On the other hand, the exponential correlation model assumes that the correlation between antenna elements decreases exponentially with the separation between them as demonstrated and verified through measurements in [19]. Consequently, we adopt the exponential channel correlation model in this study due to its compatibility with the considered massive MIMO cell model.

The transmitter and receiver correlation matrices ($\mathbf{\Phi}_t \in \mathbb{C}^{K\times K}$ and $\mathbf{\Phi}_r \in \mathbb{C}^{M\times M}$) can be defined separately. Since the UEs have only one antenna and they are sufficiently far from each other, it can be assumed that the location of the UEs do not affect the correlation directly. Accordingly, the channel correlation will only depend on the correlation

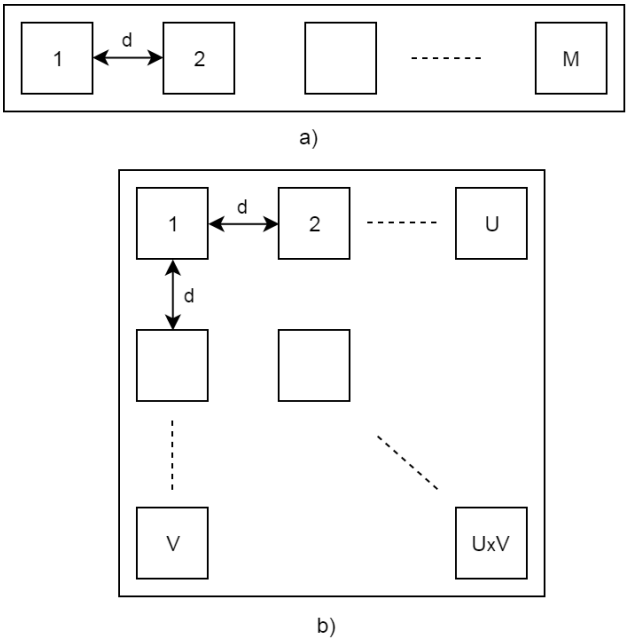

Figure 2: The considered antenna arrays in this study: (a) Uniform linear vertical (1D) and (b) uniform rectangular (2D) antenna arrays.

coefficient and the distance between antenna elements. Furthermore, since the UEs are considered to have only one antenna, there are no coupling or correlation effects in the UEs themselves. The channel correlation matrix based on the exponential correlation model is given by

$$\mathbf{\Phi} = \mathbf{\Phi}_{\mathbf{r}} = \begin{cases} \phi^{|m-n|} & m \geq n \\ (\phi^*)^{|m-n|} & m < n \end{cases} \tag{4}$$

where $(^*)$ denotes the complex conjugate and $\phi = ae^{j\theta}$ is the complex correlation coefficient, its absolute value can be between $|\phi| = 0$ (no correlation, completely independent channels) and $|\phi| = 1$ (fully correlated channels) [18]. However, this model is only suitable for $1 \times M$ uniform linear antenna arrangement (1D) as it does not consider the correlation between crosswise antenna elements. We have extended this correlation model for $U \times V = M$ elements rectangular antenna arrangements (2D) as shown in Fig. 2 (b). For a 2D antenna arrangement, the distance between two antenna elements such as m_{uv}-th and n_{uv}-th elements will be $d = \sqrt{(m_u - n_u)^2 + (m_v - n_v)^2}$, hence, the correlation matrix can be estimated by

$$\mathbf{\Phi} = \mathbf{\Phi}_r = \begin{cases} \phi^d & (m_u - n_u)^2 \geq (m_v - n_v)^2 \\ (\phi^*)^d & (m_u - n_u)^2 < (m_v - n_v)^2 \end{cases} \tag{5}$$

where the subscript $u \in U$ and $v \in V$ indicate the coordinates of the antenna element at vertical and horizontal axes of the array, respectively. Subsequently, the channel matrix including correlation can be expressed by the product of uncorrelated channel matrix $\hat{\mathbf{H}}$ and the square root of the correlation matrix $\mathbf{\Phi}$ as

$$\mathbf{H} = \hat{\mathbf{H}}\sqrt{\mathbf{\Phi}}. \tag{6}$$

In the simulations, various correlation levels with 1D and 2D antenna arrangement are considered to examine how these two arrangements impact the performance of the uplink with low-resolution ADCs.

2.4 CSI Mismatch Model

Using a specific channel estimation technique would limit the estimation errors to such a technique, therefore, to keep the CSI mismatch model generic, an additive channel estimation noise model is used as described in [17,18]. The

channel estimation error matrix $\mathbf{E}$, which consists of i.i.d. complex random variables and represents the variations from the real CSI is supposed to be independent of the $\mathbf{H}$ channel matrix. Let ρ denote the SNR given by $\rho\frac{p_u}{\sigma^2_{noise}}$. Hence, the CSI mismatch matrix will be

$$\mathbf{E} \sim \mathcal{CN}(0, \eta\boldsymbol{\Sigma}) \; and \; \eta\beta(\rho + r)^{-\alpha} \tag{7}$$

where r is a constant to make the function valid for under zero SNR values and η is the variance of the error matrix, which depends on the SNR and the two parameters $\alpha \geq 0$ and $\beta \geq 0$. $\mathcal{CN}(\mu, \boldsymbol{\Sigma})$ indicates the multivariate complex normal distribution with μ mean and $\boldsymbol{\Sigma}$ covariance matrix. By adjusting these parameters, various CSI estimation error scenarios may be obtained. For instance, if $\beta = 0$ then the perfect CSI case will be obtained. If $\alpha > 0$, the CSI estimation errors will be inversely proportional to the SNR which corresponds to that the estimation errors decrease while the SNR increases as CSI estimation is more difficult at low SNR values. If $\alpha = 0$, the estimation errors will be independent of the SNR.

Accordingly, the estimated channel matrix $\mathbf{G}$ at the BS with channel correlation and CSI estimation errors will be

$$\mathbf{G} = \hat{\mathbf{H}}\sqrt{\boldsymbol{\Phi}} + \mathbf{E}. \tag{8}$$

2.5 Data Detection

The BS estimates the channel matrix $\mathbf{G}$, which includes CSI mismatch and channel correlation effects, before performing the data detection. As non-linear receivers require high computational demands [23], a linear zero forcing (ZF) receiver is used in this study. We have also considered the maximal-ratio combining (MRC) and the minimum mean square error (MMSE) receivers, however, the performance of MRC was inferior to ZF and MMSE, and the performance of MMSE was nearly the same as ZF especially at high SNR values in line with [20]. The reason why MRC does not perform as well as others is that MRC only attempts to maximise the SNR by combining all channel gains without considering the interference between them while ZF and MMSE strive to reduce the interference between the channels as well as maximising the SNR. On the other hand, MMSE has a higher complexity than ZF as it needs the variance of the received signal power and the noise. Therefore, we have not included the results of MRC and MMSE in this study. The ZF receiver suppresses the interference between the channels using the pseudo-inverse matrix $\mathbf{W}$ of the channel matrix $\mathbf{G}$ as

$$\mathbf{W} = \mathbf{G}(\mathbf{G}^H\mathbf{G})^{-\mathbf{1}}, \tag{9}$$

where superscript ^{H} denotes the Hermitian transpose of the matrix. The ZF receiver processes quantized received baseband signals to perform the detection of UE data, thus, the received signal vector $\hat{\mathbf{x}}_\mathbf{t}$ for the t time block can be given by

$$\hat{\mathbf{x}}_t = \mathbf{W}_t^H Q_n(\mathbf{y}_t). \tag{10}$$

After recovering $\hat{\mathbf{x}}_\mathbf{t}$, M-QAM demodulation is performed to acquire the received message signal vector $\hat{\mathbf{a}}_\mathbf{t}$.

2.6 Square Root Raised Cosine Filter

Baseband communication signals have narrow-band channel characteristics. However, CSI estimation errors or channel correlation may add high-frequency noise components. Therefore, employing a low pass pulse shaping filter at the transmitter and the receiver is expected to reduce the noise injected by low-resolution quantization as well as the inter-channel interference. One of the most common type of such filters used in communication systems is the square root raised cosine filter (SRRC) due to its ease of implementation and ability to reduce the inter-channel interference. The SRRC filter shapes the pulses as sinc functions in the time domain to reduce their bandwidths. This filter is usually used as a matched filter pair which comprises of two identical SRRC filters which are implemented at the transmitter and the receiver. The frequency response of these two filters jointly reaches a raised cosine (RC) filter‘s frequency response. The transfer function of the SRRC is given [24, 25] by

$$H(f) = \begin{cases} \sqrt{T} & |f| < \omega_0 \\ \sqrt{\frac{T}{2}\Big[1 - sin(\frac{\pi T}{\delta}(|f| - \omega_1))\Big]} & \omega_0 < |f| < \omega_1 \\ 0 & |f| > \omega_1 \end{cases} \tag{11}$$

where $\omega_0 = \frac{1-\delta}{2T}$ and $\omega_1 = \frac{1+\delta}{2T}$ and $0 < \delta < 1$ is the roll-off factor which determines the excess bandwidth of the filter. Higher roll-off factors allow higher excess bandwidths over the Nyquist bandwidth of the signal. When $\delta = 0$, the filter would have very sharp frequency response without having any excess bandwidth, however, this is extremely difficult to implement as it would require a great number of filter taps. For this reason, the roll-off factor is typically selected between $0.2 - 0.4$ in communication systems to allow a smooth filter response [25]. In this study, an SRRC filter with $\delta = 0.3$ roll-off factor is implemented at the UEs and the BS to limit the bandwidth of each channel to reduce the interference between them. Moreover, it also reduces the quantization noise and channel estimation errors according to the results of this study.

3 Uplink Achievable Upper Bound

In this section, we derive the upper bound of the ZF receiver under CSI mismatch and the distortion caused by low-resolution ADCs. Various expressions have been derived to estimate the data rate of the low-resolution quantized uplink [11], [26] and [27]. These expressions rely on the channel $\mathbf{H}$, message signals and noise components be randomly and independently varying depending on the related probability functions. The additive quantization noise model (AQNM) is employed in [26] and the pseudo-quantization noise (PQN) model is employed in [27] to approximate the noise and the distortion caused by low-resolution ADCs. Both quantization error models have similar impacts on the performance [26], hence, PQN is used in this study to estimate the quantization distortion and noise.

In order to calculate the achievable rate (upper bound), firstly the constituents of the received signal must be shown explicitly. The output of the ZF receiver can be expressed by (12) in which $\mathbf{\Psi}_i$ is the corresponding error matrix after the ZF receiver due to the channel correlation and the CSI mismatch. $\mathbf{w_k^H}$ denotes the kth column of the receiver matrix for the kth UE. I_1 denotes the interference which is caused by the other UEs in the case of perfect CSI, which is negligible as the ZF receiver strives to cancel it out. However, interference I_2, which is induced by the CSI mismatch, has a significant impact on the data rate, hence, this must be taken into account.

$$\hat{x}_k = \underbrace{\sqrt{p_u}\mathbf{w}_k^H\mathbf{h}_k x_k}_{desired\ signal} + \underbrace{\sqrt{p_u}\sum_{i=1,i\neq k}^{K}\mathbf{w}_k^H\mathbf{h}_i x_i}_{I_1} + \underbrace{\sqrt{p_u}\sum_{i=1}^{K}\mathbf{\Psi}_i\mathbf{w}_k^H\mathbf{h}_i x_i}_{I_2} + \mathbf{w}_k^H\mathbf{n} + \mathbf{n}_q \tag{12}$$

It is assumed that the noise and interference induced by imperfect CSI has a linear correlation with the noise factor (η) and the SNR ρ due to (7). The relation between the CSI error matrix $\mathbf{E}$ and $\mathbf{\Psi}$ can be expressed as $\mathbf{\Psi} = z\mathbf{E}$, then each element of $\mathbf{\Psi}$ can be estimated as a Gaussian random variable which is given by $\psi_{mk} \sim \mathcal{N}(0, \beta(\rho + r)^{-\alpha})$. In this way, the noise induced by the CSI mismatch can be estimated.

According to the Shannon capacity equation, the capacity of the communication links is related to the SNR as

$$R_k = \log_2(1 + SNR). \tag{13}$$

The received signal is substantially impaired by AWGN channel noise, interference, channel estimation errors and quantization noise because of low-resolution ADCs. Therefore, SINQR is used instead of SNR in this study. SINQR denotes the signal to total noise, interference and quantization noise ratio.

Let $\mathbf{n_q}$ denote the quantization noise and the distortion vector caused by low-resolution ADCs and $\mathbf{w}_k$ denote the kth column of the receiver filter $\mathbf{W}$, the average total noise power before quantization is given by

$$\Sigma P_N = p_u \sum_{i=1,i\neq k}^{K}\mathbb{E}[|\mathbf{w}_k^H\mathbf{h}_i|^2] + p_u\sum_{i=1}^{K}\mathbb{E}[|\mathbf{\Psi}_i\mathbf{w}_k^H\mathbf{h}_i|^2] + \mathbb{E}[|\mathbf{w}_k^H\mathbf{n}|^2]. \tag{14}$$

Subsequently, the total post quantization noise power can be calculated as $\Sigma P_N + \mathbb{E}[|\mathbf{n}_q|^2]$ by adding the quantization noise power $\mathbb{E}[|\mathbf{n}_q|^2]$. The quantization induces a noise and a non-linear distortion $\mathbf{n}_q$ which is caused by the limited

resolution of the ADCs. To solve this equation, the expected value of quantization noise and distortion is required and it is given in [27] with the PQN model as

$$\mathbb{E}\{|\mathbf{n}_q|^2\} = \frac{1}{3}\left(p_u \sum_{i=1}^{K} \gamma_k + \Sigma P_N\right)(\theta_0 + \theta_1 n)2^{-2n} \tag{15}$$

.

where γ_k is the path-loss and the shadowing related large-scale fading coefficient. $(\theta_0 + \theta_1 n)2^{-2n}$ indicates the quantization distortion depending on the ADC resolution $n = \{1, 2, 3, 4\}$-bit, is calculated numerically in [22]. These ADC distortion factors are obtained as $\theta_0 = 16$ and $\theta_1 = 12$ for 1-bit ADCs, and $\theta_0 = 4$ and $\theta_1 = 7$ for 2-bit and 3-bit ADCs. ADCs are assumed to have perfect automatic gain control units, hence, the received signals have been amplified perfectly to fit the ADC range and are not clipped. Consequently, the SINQR can be calculated as

$$SINQR = \frac{p_u \mathbb{E}[|\mathbf{w}_k^H \mathbf{h}_k|^2]}{\Sigma P_N + \mathbb{E}[|\mathbf{n}_q|^2]}. \tag{16}$$

The estimated SINQR by (16) and can be substituted in the generic ZF capacity equation to find the upper bound of the uplink. Achievable capacity limit of ZF is given by

$$R_{ZF} = \log_2(1 + SINQR(M - K + 1)) \tag{17}$$

Substituting (14) and (15) in (16), and then in (17), the upper bounded achievable capacity is obtained as

$$R_{ZF} = \log_2\left(1 + \frac{p_u(M - K + 1)}{\Sigma P_N + \frac{1}{3}(p_u \sum\limits_{i=1}^{K} \gamma_k + \Sigma P_N)(\theta_0 + \theta_1 n)2^{-2n}}\right). \tag{18}$$

This upper bound approximation, which takes CSI mismatch, quantization noise, interference into account, has been computed and verified using Monte-Carlo simulations in the numerical results section below.

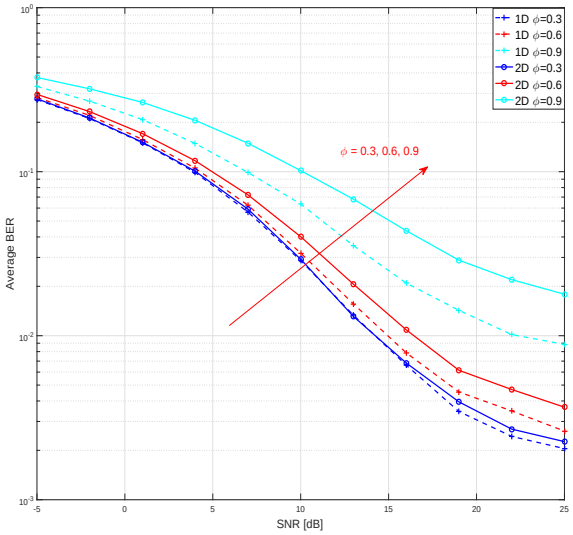

Figure 3: Average BER as a function of SNR for 1D and 2D antenna arrangement with different channel correlation (ϕ) coefficients ($M = 100$ BS Antennas, $K = 10$ UEs, 64QAM, 3-bit ADCs and perfect CSI).

Table 1: The system parameters used in the simulations.

Parameter	Description	Value
R	cell radius	2000 m
M	number of BS antennas	100
$U \times V$	rectangular array elements	10×10
K	number of UEs	10
v	path loss exponent	4
δ	SRRC roll-off factor	0.3
σ_{shadow}	shadowing factor	6 dB
ϕ	channel correlation coefficient	$0 < \phi < 1$
α and β	CSI mismatch coefficients	$\alpha = 1.5$ and $\beta = 15$
BW	total channel bandwidth	200 MHz
f_S	ADC sampling rate	800 MS/s
n	ADC resolution	1, 2, 3, 4-bit

4 Numerical Results

Monte-Carlo simulation is used to examine the joint impact of the channel correlation and the CSI mismatch. In the generic system model, the massive MIMO network under consideration consists of a BS with $M = 100$ antennas and $K = 10$ UEs, unless stated otherwise. The UEs are randomly located around the BS in a circular cell within 2000 m distance. The large-scale fading of each UE, γ_k, which is a log-normal distributed random variable with the distance between the BS and the kth UE, is given by $\gamma_k = r_k/d_k^v$ where the $v = 4$ denotes the path loss exponent and r_k is the random log-normal shadowing with $\sigma_{shadow} = 6$ dB. The non-correlated channels between the BS and the UEs are assumed to be non-line-of-sight (NLOS), therefore, the small-scale fading coefficients, $f_m k$, are random variables with the Rayleigh distribution. However, for the correlated channels, which have strong line-of-sight (LOS) components, the correlation levels are induced by the channel correlation coefficient ϕ. Table 1 presents the list of the general network parameters used in the simulations.

In this study, bit error rate (BER) and average mutual information (MI) are used as performance metrics. The spectral efficiency between the kth UEs and the BS can be estimated by calculating the MI between the transmitted data vector $\mathbf{a}_k$ and the received data vector $\hat{\mathbf{a}}_k$ as

$$I(\mathbf{a}_k; \hat{\mathbf{a}}_k) = \sum_{a_k \in \mathbf{a}_k} \sum_{\hat{a}_k \in \hat{\mathbf{a}}_k} p(a_k, \hat{a}_k) \log \frac{p(a_k, \hat{a}_k)}{p(a_k)p(\hat{a}_k)} \tag{19}$$

where $p(a_k)$ denotes the marginal probability mass function of a_k. $p(a_k, \hat{a}_k)$ denotes the joint probability mass function of the transmitted and the received data, which designates the probability of the correctly transmitted information between the transmitter and the receiver. Hence, if all information is transmitted correctly (i.e. BER=0), the MI will be equal to the maximum capacity of the modulation scheme, otherwise, having transmission errors will reduce the MI. As there is no closed form for these probability mass functions under the aforementioned channel conditions and modulation schemes, these functions are obtained from the transmitted and the received data.

Randomly generated binary messages are modulated using QPSK or M-QAM by the UEs as described in section 2. Subsequently, these modulated symbols are transmitted to the BS through the channel $\mathbf{H}$. On the receiver side, the received signals including noise and the interference are quantized and then processed by the ZF receiver. QPSK, 16QAM, 32QAM, or 64QAM modulated uplinks, which are quantized using 1-bit to 3-bit ADCs, have been considered here. The SRRC filters with $\delta = 0.3$ roll-off factor are designed as finite impulse response (FIR) filters and employed at the UEs and the BS to shape the baseband transmitted and received signals and limit their bandwidths as described in subsection 2.6. All scenarios are repeated 100000 times and the average values are presented in the figures.

Firstly, the impact of the 1D (1×100 elements) and the 2D (10×10 elements) antenna arrangements on the BER is examined. Fig.3 illustrates the BER of 64QAM modulated uplink with 3-bit ADCs as a function of SNR using aforementioned antenna arrangements. In this network setup, the BS has the perfect CSI and utilises the SRRC. The 2D antenna arrangement led to significantly higher BER due to the fact that the rectangular antenna placement causes more correlation among antenna elements. However, the 2D antenna arrangement is more practical in applications of massive MIMO because of the limited space of the BS. The performance difference between these two antenna arrangements become more significant at higher correlation coefficients ϕ and higher SNR values. After observing the impact of

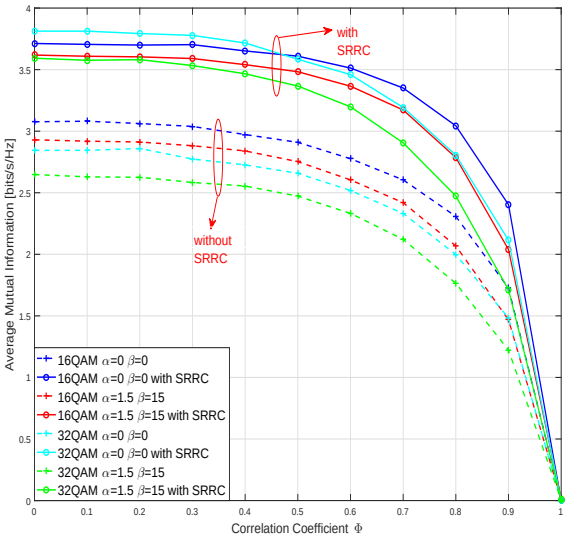

Figure 4: The impact of the correlation on the mutual information of the uplink. (2-bit ADCs, $M = 100$, $K = 10$ $SNR = 5dB$).

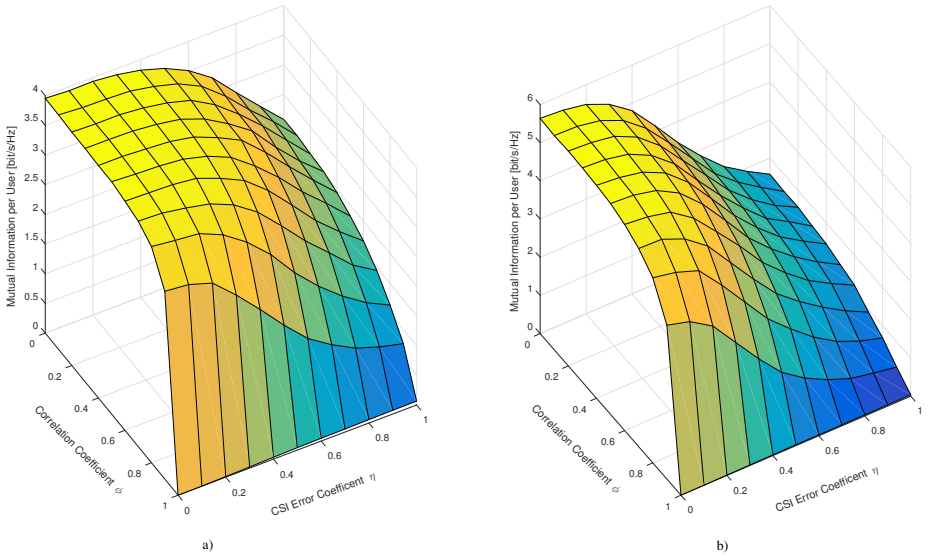

Figure 5: The joint impact of the channel correlation and the CSI mismatch on the mutual information per user for; (a) 16QAM uplink with 2-bit ADCs, (b) 64QAM uplink with 3-bit ADCs (M=100, K=10, SNR=10 dB and with the SRRC filter).

the antenna placements on the BER, only the 2D antenna arrangement model is used in the subsequent analysis as it provides a more realistic approach for a BS antenna array.

Fig. 4 illustrates how the correlation increase affects the mutual information with and without perfect CSI in 2-bit quantized system. The uplink of each UE is modulated using 16QAM and 32QAM and the received SNR on each antenna element is 5dB. The CSI mismatch is represented by α and β coefficients as explained before. For instance, the perfect CSI case is obtained with $\alpha = 0$ and $\beta = 0$. This figure shows that the SRRC filter significantly dampens the noise effects and enhances the spectral efficiency in all cases. Therefore, in the following simulations, the SRRC filter is always assumed to be implemented. As seen in the figure, up to $\phi \leq 0.5$ correlation, its impact on the system is

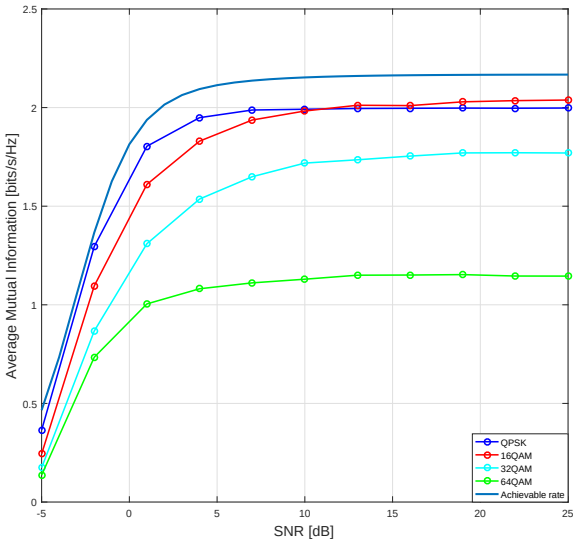

Figure 6: The joint impact of a moderate level channel correlation ($\phi = 0.6$) and CSI estimation errors with 1-bit ADCs on the mutual information. ($M = 100$, $K = 10$).

limited, therefore this region can be considered as low correlation region. The middle level correlation can be defined as $0.5 \leq \phi \leq 0.7$, and high level correlation region is defined as $\phi \geq 0.7$ according to their impact on the uplink mutual information.

It is important to consider the joint impact of the correlation and the CSI mismatch as both of them may vary over a wide range in a real system application. Hence, they are assumed to vary between 0 and 1. The joint impact is presented in Fig. 5 in which 16QAM and 64QAM modulated uplinks are considered with 2-bit and 3-bit ADCs, respectively. Although, the 64QAM uplink is quantized by 3-bit ADCs, its performance is degraded further by the correlation and the CSI mismatch. The impact of the low correlation ($\phi \leq 0.5$) is not significant. However, a high correlation e.g. $\phi > 0.7$ significantly degrades the mutual information. On the other hand, even a small amount of CSI mismatch may degrade the performance significantly.

In the next analysis, the performance of 1-bit, 2-bit and 3-bit ADCs are compared with various modulation schemes, in which moderate values for the correlation $\phi = 0.6$ and CSI errors ($\alpha = 1.5$ and $\beta = 15$) have been used to, on average, represent a realistic channel conditions for a massive MIMO application. Fig. 6. presents the average mutual information of 1-bit quantized system with various modulation schemes and compares them to the achievable capacity. Under 1-bit quantization, only QPSK can achieve its capacity (2 bits/Hz) through a correlated channel with CSI mismatch. The demodulation of higher order modulation schemes such as 16QAM, 32QAM and 64QAM could not be performed effectively due to the quantization distortion caused by 1-bit quantization. Therefore, it can be seen that 1-bit quantization is only suitable for QPSK modulated communication links under these channel conditions. Fig. 7. presents the average mutual information of 2-bit quantized system, in which 16QAM achieves its capacity (4 bits/Hz) in addition to QPSK. 32QAM and 64QAM modulated uplinks can reach similar spectral efficiencies to 2-bit ADCs, however they cannot achieve their capacity limits even at high SNR values. Fig. 8. displays the average mutual information of the same modulation schemes with 3-bit ADCs. This figure shows that 3-bit ADCs can provide enough resolution for performing 64QAM. It should be noted here, the increased resolution by only 1-bit has provided significant performance improvement as can be seen from the comparison among Fig. 6., Fig 7 and Fig. 8.

The comparison of the aforementioned scenarios which employ 1-bit, 2-bit and 3-bit ADCs under realistic network scenarios including various channel correlations and CSI mismatches shows that the feasible modulation schemes for the uplink are mainly limited by the resolution of ADCs. For example, 1-bit resolution is suitable for QPSK, however, it does not provide enough data for the demodulation of 16QAM. Furthermore, they show that coarse quantization makes the network more sensitive to the channel correlation and the CSI mismatch.

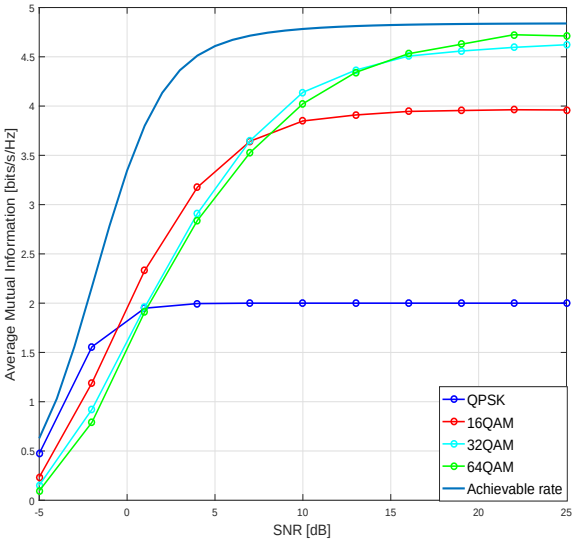

Figure 7: The joint impact of a moderate level channel correlation ($\phi = 0.6$) and CSI estimation errors with 2-bit ADCs on the mutual information. ($M = 100$, $K = 10$).

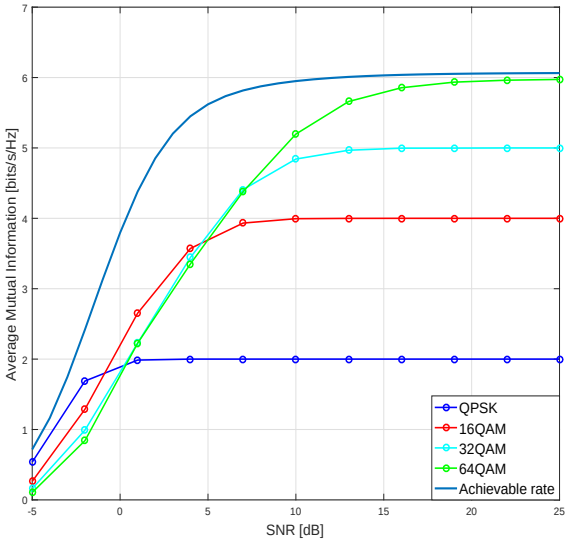

Figure 8: Combined effects of a moderate level channel correlation ($\phi = 0.6$) and CSI estimation errors with 3-bit ADCs on the mutual information. ($M = 100$, $K = 10$).

Table 2: The required minimum energy levels per conversion of ADCs which operate at 800 MS/s rate with different resolutions .

	1-bit	2-bit	3-bit	4-bit
Bit/Joule $\times 10^{-5}$	2.4594	8.2766	21.4082	50.3663

In addition to the performance of low-resolution ADCs, their energy efficiency is examined using theoretical power consumption limits of the ADCs. 350 nm CMOS pipeline ADC architecture is considered. Its energy consumption limits per conversion P_A is given in [27, 28] by

$$P_A = P_{noise} + (2^n - 1)\left(1 + 2n \cdot ln2 \frac{V_{eff}}{V_D}\right) C_{min} V_D^2 f_s. \tag{20}$$

where the parameters are $V_D = 3$ V, $V_{eff} = 300$ mV, $C_{min} = 3$ fF and $P_{noise} = 100$ fJ for process limited 300nm ADCs [28]. The sampling rate of the ADCs is assumed to be $f_s = 800$ MS/s as a millimetre-wave channel with 200 MHz bandwidth is considered, which requires 4 sample per symbol during the quantization. Table 2 gives how much energy required per conversion with regard to resolution of ADCs. It must be noted here, there are 200 ADCs at the BS, hence these values must be multiplied by 200 to calculate the total energy consumption of the ADC block for each conversion. To make a fair comparison between different resolutions in terms of energy efficiency, we have selected the optimum modulation schemes for each resolution. Although high resolution ADCs consume more energy, they can be used in the demodulation of higher order modulation schemes. Therefore, QPSK modulation is used in the 1-bit quantized system, 16QAM is used in the 2-bit quantized system, 32QAM and 64QAM are used in the 3-bit quantized system and 64QAM is used in the 4-bit quantized system. Although a moderate level channel correlation case ($\phi = 0.6$) have been investigated in Fig. 6-8, to show the impact of a higher level correlation on the energy efficiency of the ADCs, ($\phi = 0.8$) is selected in this section. Each network setup has a CSI mismatch which is set by $\alpha = 1.5$ and $\beta = 15$. 1-bit QPSK modulated uplink without any correlation and with perfect CSI (perfect channel conditions) has been also considered for the comparison and it is indicated by 'QPSK Perfect' in the figures.

Figure 9 (a) illustrates the spectral efficiency of the uplink with low-resolution ADCs and Figure 9 (b) illustrates the required energy for ADC blocks (200 ADCs) with regard to ADC resolution. Each modulation scheme is quantized with the appropriate ADC resolution i.e. QPSK with 1-bit quantization, 16QAM with 2-bit quantization etc. According to this figure, although, the capacity of the 1-bit system is limited by 2 bit/Hz/s due to QPSK, it is the most energy efficient because of low energy consumption of 1-bit ADCs. Therefore, QPSK with 1-bit quantization can be considered for the systems which need a robust communication link but not a high throughput such as wireless sensor networks or internet of things networks. This would decrease their energy consumption and reduce the complexity of the hardware and the algorithms. Figure 9 also shows how the channel correlation and CSI mismatch reduces the energy efficiency of the system especially in the low SNR regions as seen from the comparison between two QPSK modulated system with a perfect channel and impaired channel. As expected, 4-bit ADCs has the lowest energy efficiency. For example, 3-bit ADCs can double the energy efficiency of the system in comparison to the 4-bit quantized uplink while providing a reasonable performance.

5 Conclusion

In this study, the joint impact of the channel correlation and the CSI mismatch on quantized massive MIMO systems with the ZF has been investigated in terms of spectral efficiency and energy efficiency. Furthermore, an analytical upper bound expression for the capacity of the ZF under the aforementioned conditions is derived. QPSK to 64QAM uplinks with 1-bit, 2-bit and 3-bit ADCs are examined under realistic channel conditions. According to the results, channel correlation and CSI mismatch significantly degrade the spectral efficiency of the low-resolution ADC systems under consideration, prompting the need to carefully select appropriate modulation schemes to match the low-resolution ADCs such that acceptable trade-off between spectral and energy efficiencies can be achieved.

References

[1] Larsson, E.G., Edfors, O., Tufvesson, F. and Marzetta, T.L.: 'Massive MIMO for next generation wireless systems', IEEE communications magazine, 2014, 52(2), pp.186-195.

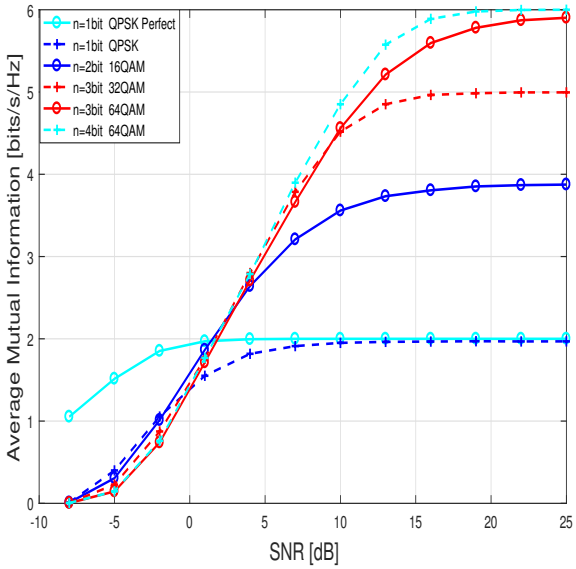

(a)

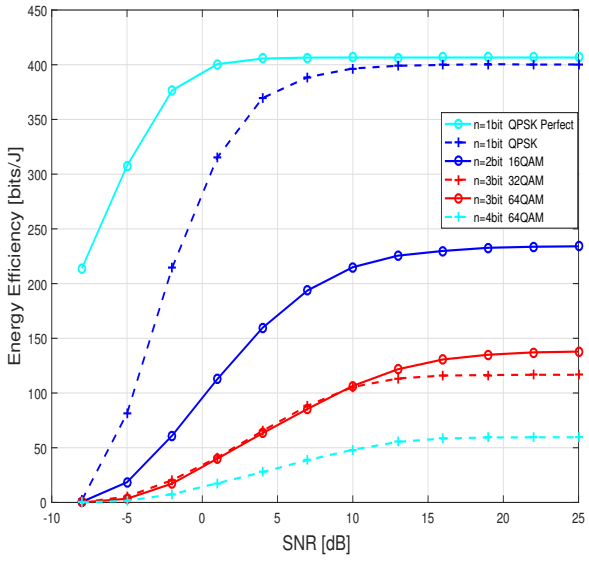

(b)

Figure 9: The impact of the low-resolution ADCs on spectral efficiency and energy efficiency. (a) Spectral efficiency and (b) Required energy consumption per bit data for ADCs under a high channel correlation ($\phi = 0.8$) and CSI estimation errors ($\alpha = 1.5$ and $\beta = 15$). ($M = 100$, $K = 10$).

[2] Mollen, C., Choi, J., Larsson, E.G., et al.: 'Uplink performance of wideband massive MIMO with one-bit ADCs', IEEE Trans. Wirel. Commun., 2017, 16, (1), pp. 87–100

[3] Halsig, T., Lankl, B.: 'Spatial oversampling in LOS MIMO systems with 1-bit quantization at the receiver'. Proc. 11th Int. ITG Conf. on Systems, Communications and Coding (SCC 2017), Hamburg, Germany, 2017, pp. 1–6

[4] Jacobsson, S., Durisi, G., Coldrey, M., et al.: 'One-bit massive MIMO: channel estimation and high-order modulations'. IEEE Int. Conf. on Communication Workshop, London, UK, 2015, pp. 1304-1309.

[5] Risi, C., Persson, P., Larsson, E.G.: 'Massive MIMO with 1-bit ADC', arXiv preprint arXiv:1404.7736, 2014.

[6] Choi, J., Mo, J., Heath, R. W.: 'Near maximum-likelihood detector and channel estimator for uplink multiuser massive MIMO systems with one-bit ADCs', IEEE Trans. Commun., 2016, 64, (5), pp.2005-2018.

[7] Li, Y., Cheng, T., Seco-Granados, G., et al.: 'Channel estimation and performance analysis of one-bit massive MIMO systems', IEEE Trans. Signal Process., 2017, 65, (15), pp.4075-4089.

[8] Le, B., Rondeau, T.W., Reed, J.H., et al.: 'Analog-to-digital converters', IEEE Signal Process. Mag., 2005, 22, (6), pp.69-77.

[9] Hoyos, S., Sadler, B.M., Arce, G.R.: 'Monobit digital receivers for ultrawideband communications', IEEE Trans. Wirel. Commun., 2005, 4, (4), pp.1337-1344.

[10] O'Donnell, I.D., Brodersen, R.W.: 'An ultra wideband transceiver architecture for low power, low rate, wireless systems', IEEE Trans. Veh. Technol., 2005, 54, (5), pp.1623-1631.

[11] Jacobsson, S., Durisi, G., Coldrey, M., *et al.*: 'Throughput analysis of massive MIMO uplink with low-resolution ADCs', IEEE Transactions on Wireless Communications, 2017, 16, (6), pp.4038-4051.

[12] Gauger, M., Hoydis, J., Hoek, C., et al.: 'Channel measurements with different antenna array geometries for massive MIMO systems'. Proc. 10th Int. ITG Conf. on Systems, Communications and Coding (SCC 2015), Hamburg, Germany, 2015, pp. 1-6.

[13] Chen, X.: 'Antenna correlation and its impact on multi-antenna system', Prog. Electromagn. Res. B, 2015, 62, pp.241-253.

[14] Masouros, C., Sellathurai, M., Ratnarajah, T.: 'Large-scale MIMO transmitters in fixed physical spaces: the effect of transmit correlation and mutual coupling', IEEE Trans. Commun., 2013, 61, (7), pp.2794-2804.

[15] Ying, D., Vook F.W., Thomas, T.A., *et al.*: 'Kronecker product correlation model and limited feedback codebook design in a 3D channel model'. 2014 IEEE Int. Conf. on Communications (ICC), Sydney, NSW, Australia, 2014, pp. 5865–5870.

[16] Mi, D., Dianati, M., Zhang, L., et al.: 'Massive MIMO performance with imperfect channel reciprocity and channel estimation error', IEEE Trans. Commun., 2017, 65, (9), pp.3734-3749.

[17] Aquilina, P., Ratnarajah, T.: 'Performance analysis of IA techniques in the MIMO IBC with imperfect CSI', IEEE Trans. Commun., 2015, 63, (4), pp.1259–1270.

[18] Nauryzbayev, G., Alsusa, E., Abdallah, M.: 'On the feasibility of interference alignment in compounded MIMO broadcast channels with antenna correlation and mixed user classes', IEEE Trans. Veh. Technol., 2018, 67, (3), pp.2130-2140.

[19] Gao, X., Edfors, O., Rusek, F., *et al.*: "Massive MIMO performance evaluation based on measured propagation data", IEEE Trans. Wirel. Commun., 2015, 14, (7), pp.3899-3911.

[20] Ngo, H.Q., Larsson, E.G., Marzetta, T.L.: "Energy and spectral efficiency of very large multiuser MIMO systems", IEEE Trans. Commun., 2013, 61, (4), pp.1436-1449

[21] Liu, L., Matolak, D. M., Tao, C., *et al.*: 'Sum-rate capacity investigation of multiuser massive MIMO uplink systems in semi-correlated channels'. Vehicular Technology Conf. (VTC Spring), Nanjing, China, 2016, pp. 1-5.

[22] Hoydis, J., Hoek, C., Wild, T., *et al.*: 'Channel measurements for large antenna arrays', 2012 International Symposium on Wireless Communication Systems (ISWCS), Paris, 2012.

[23] Rico, U. P., Alsusa, E., Masouros, C.: 'A Fast Least-Squares Solution-Seeker Algorithm for Vector-Perturbation', IEEE GLOBECOM 2008 - 2008 IEEE Global Telecommunications Conference, New Orleans, 2008.

[24] Chia-Yu, Y., Chien, C.: 'Design of a square-root-raised-cosine FIR filter by a recursive method'. IEEE Int. Symp. on Circuit Systems (ISCAS 2005), Kobe, Japan, 2005, pp. 512-515.

[25] Tranter, W.H., Rappaport, T.S., Kosbar, K.L., *et al.*: 'Principles of communication systems simulation with wireless applications'. (New Jersey: Prentice Hall, 2004)

[26] Zhang, J., Dai, L., Sun, S. *et al.*: 'On the spectral efficiency of massive MIMO systems with low-resolution ADCs', IEEE Communications Letters, 20(5), 2016, pp.842-845.

[27] Sarajlic, M., Liu, L. and Edfors, O.: 'When are low resolution ADCs energy efficient in massive MIMO?'. IEEE Access, 2017, 5, pp.14837-14853.

[28] Sundstrom, T., Murmann, B., Svensson, C.: 'Power dissipation bounds for high-speed nyquist analog-to-digital converters', IEEE Trans. Circuits Syst., 2009, 56, (3), pp.509-518.